THE ASTROPHYSICAL JOURNAL, 416:137–149, 1993 October 10

THE LYMAN-ALPHA FOREST OF PKS 2126−158 AT HIGH RESOLUTION[1]

EMANUELE GIALLONGO
Osservatorio Astronomico di Roma, via dell' Osservatorio, I-00040 Monteporzio, Italy
STEFANO CRISTIANI
Dipartimento di Astronomia, Università di Padova, vicolo dell' Osservatorio 5, I-35122 Padova, Italy
ADRIANO FONTANA
Dipartimento di Fisica, II Università di Roma, via E. Carnevale, I-00173 Roma, Italy
AND
DARIO TRÈVESE
Istituto Astronomico, Università di Roma " La Sapienza," via G. M. Lancisi 29, I-00161 Roma, Italy
Received 1992 December 23; accepted 1993 April 21

ABSTRACT

The spectrum of the quasar PKS 2126−158 ($z_{em} = 3.27$) has been observed at the resolution of 14 km s^{-1} in the wavelength interval 4750–7000 Å. We give a list of Lyα absorption lines and metal-line systems. Column densities N and Doppler widths b are derived by a fitting procedure. Velocity structures up to 300 km s^{-1} are found in the strongest C IV doublets. Although selection effects could explain the observed b-N_{HI} correlation for the Lyα lines, an intrinsic deficit of strong lines with low b values is present in our spectrum. The present data have been merged with other high-resolution data available in the literature to determine the overall column density distribution. A simple power-law fit $N_{HI}^{-\beta}$ gives $\beta = 1.7$; however, a better description of the data is obtained with a flatter power law with $\beta = 1.5$ and a break at log $N_{HI} \sim 15$, a feature predicted by some theoretical Lyα cloud models. A new analysis of the proximity effect gives a UV background flux 7×10^{-22} ergs s^{-1} cm^{-2} Hz^{-1} sr^{-1}, not far from the integrated quasar contribution.

Subject headings: intergalactic medium — quasars: absorption lines — quasars: individual (2126−158)

1. INTRODUCTION

The spectra of quasars shortward of the Lyα emission show a crowd of narrow absorptions due mainly to Lyman-α lines caused by intervening clouds along the line of sight (Lynds 1971; Sargent et al. 1980). Only a small fraction of the lines is due to elements heavier than hydrogen.

The knowledge of the physical and cosmological properties of the Lyα absorbers relies on a few parameters which can be derived from high-resolution spectroscopy.

Information on the physical condition within the clouds can be obtained from column densities and Doppler widths of the absorption lines, by Voigt profile fitting, once some assumptions are made on the ionizing background flux and the observational constraints on the cloud sizes are taken into account.

The redshift distribution of the clouds provides information on their cosmological evolution and their clustering properties. General results on the physical and cosmological properties of the absorbing clouds have been obtained through large samples of lines ($\simeq$1000 lines from $\simeq$40 QSOs) derived from intermediate-resolution spectroscopy (see, e.g., Murdoch et al. 1986; Lu, Wolfe, & Turnshek 1991). However, blending effects, which are relevant at this resolution, can affect the determination of the intrinsic properties and the evolution of the Lyα population (see, e.g., Liu & Jones 1988; Giallongo 1991; Trèvese, Giallongo, & Camurani 1992).

High-resolution spectroscopy ($R > 20{,}000$) reduces spurious effects and allows profile fitting of the lines, but high-resolution spectra with sufficient wavelength coverage and signal-to-noise ratio have been obtained for only a few objects.

Typical values of the neutral hydrogen column density and Doppler width seem to depend on the deblending procedures and the contamination of very narrow and weak metal lines in the Lyα forest. Some authors indicate typical values $N_{HI} \sim 10^{13-14}$ atoms cm^{-2} and $b = 30$ km s^{-1} (Carswell et al. 1984, 1987, 1991; Rauch et al. 1992) corresponding, under the assumption of pure thermal broadening, to $T_c \sim 5 \times 10^4$ K. However, Pettini et al. (1990) claim typical b values as low as $b = 17$ km s^{-1} and a tight correlation between b and N_{HI} parameters which suggests lower temperatures ($T \lesssim 10^4$ K) and would imply a further important constraint on the physics of the clouds.

The most recent and accurate estimate of the cloud sizes has been obtained by Smette et al. (1992) from the spectra of a gravitationally lensed high-redshift quasar UM 673 ($z_{em} = 2.7$). They derive lower and upper limits of 12 h_{50}^{-1} kpc and 160 h_{50}^{-1} kpc, respectively, for the diameter of spherical clouds, or 24 kpc and 320 kpc, for oblate spheroids with an axis ratio <0.1.

In this way, assuming a cloud temperature of 3×10^4 K, gravitational energy is overwhelmed by thermal energy and the clouds have to be confined by a hotter and highly ionized, diffuse IGM unless nonbaryonic dark matter contributes appreciably to the gravitational potential of the clouds.

In any case, part of the gas should be at temperature $T \lesssim 2 \times 10^4$ K ($b < 20$ km s^{-1}) in clouds which cannot be in thermal and ionization equilibrium, being at the same time pressure or gravitationally confined, as pointed out by Chaffee et al. (1983) and Carswell et al. (1984). Adiabatic expansion of the clouds has been invoked to explain such low temperatures (Duncan, Vishniac, & Ostriker 1991; Petitjean et al. 1993).

The ionization of the IGM can be constrained by the absence of the long-sought absorption trough shortward of the

[1] Based on material collected at the ESO-La Silla Telescopes.

QSO Lyman-α emission (GP test; see Gunn & Peterson 1965). The most recent estimate is $\tau_{GP} = 0.013 \pm 0.026$ at $z = 3$ (Giallongo, Cristiani, & Trèvese 1992b).

Considering that the ionized UV background flux (UVB) produced by the quasar population at $z = 2$–3, $J \sim 10^{-22} J_{-22}$ ergs cm^{-2} s^{-1} Hz^{-1} sr^{-1} (Bechtold et al. 1987; Madau 1992) keeps both the clouds and IGM ionized, the physical state and evolution of the diffuse IGM can be further constrained under the assumption that clouds are pressure confined (Sargent et al. 1980; Ostriker & Ikeuchi 1983; Steidel & Sargent 1987; Giallongo et al. 1992a).

A greater sample of Lyα lines obtained from high-resolution spectra can establish the fraction of low-temperature absorbers and their cosmological evolution. To this purpose, we present a high-resolution spectrum ($R = 22{,}000$) of the quasar PKS 2126−158 at $z = 3.27$, extending from 4750 to 7000 Å, and give information on the temperature and the column density distributions of the clouds. Consequences on the estimate of the ionizing UVB are discussed.

2. DATA ACQUISITION AND REDUCTION

The quasar PKS 2126−158 has been observed at ESO (La Silla) in 1991 August, with the NTT telescope and the EMMI instrument in the echelle mode (see D'Odorico 1990). Two spectra of 7200 s each were obtained on August 6, and one of 9130 s on August 7. The slit was 1″.5 wide, and the seeing always less or equal to 1″. Particular attention was paid in order to minimize the effects of the atmospheric dispersion. The absolute flux calibration was carried out by observing the standard star EG 274 (Stone & Baldwin 1983). The data reduction has been carried out using the standard echelle package described in the 1991 November edition of the MIDAS software (Banse et al. 1988). Wavelengths have been corrected to vacuum heliocentric values, and fluxes have been dereddened for galactic extinction according to the Savage & Mathis (1979) curves. A value of $E_{B-V} = 0.04$ has been assumed on the basis of the Burstein & Heiles maps (1982). The weighted mean of the spectra has been obtained at the resolution $R = 22{,}000$ after rebinning at uniform $\Delta\lambda$ close to the original sampling. The signal-to-noise ratio ranges from 6 to 12 in the interval 4700–7000 Å.

3. THE DETECTION AND MEASURE OF ABSORPTION LINES

As usual, a local continuum has been determined selecting regions free of strong absorption lines, where the rms fluctuation about the mean becomes consistent with noise statistics (see Young et al. 1979). A smoothed continuum has been obtained using spline fits to these spectral regions. The spectrum has then been normalized to the continuum and the observed portion of the Lyα forest is shown in Figure 1, while Figures 2*a* and 2*b* show the spectrum longward of the Lyα emission.

The detection of absorption lines in the spectrum has been performed as follows:

1. In regions of the normalized continuum with uniform signal-to-noise ratio we have computed the histogram of the pixel intensities. In general, the intensity distribution in the Lyα forest is skewed toward lower values, due to the presence of absorption lines.
2. A Gaussian profile to the high-intensity side of the histogram is fitted, starting from the maximum of the intensity distribution: the variance obtained is taken as a conservative estimate of the noise level in the region considered.
3. All the lines whose central relative intensity is 3 σ below

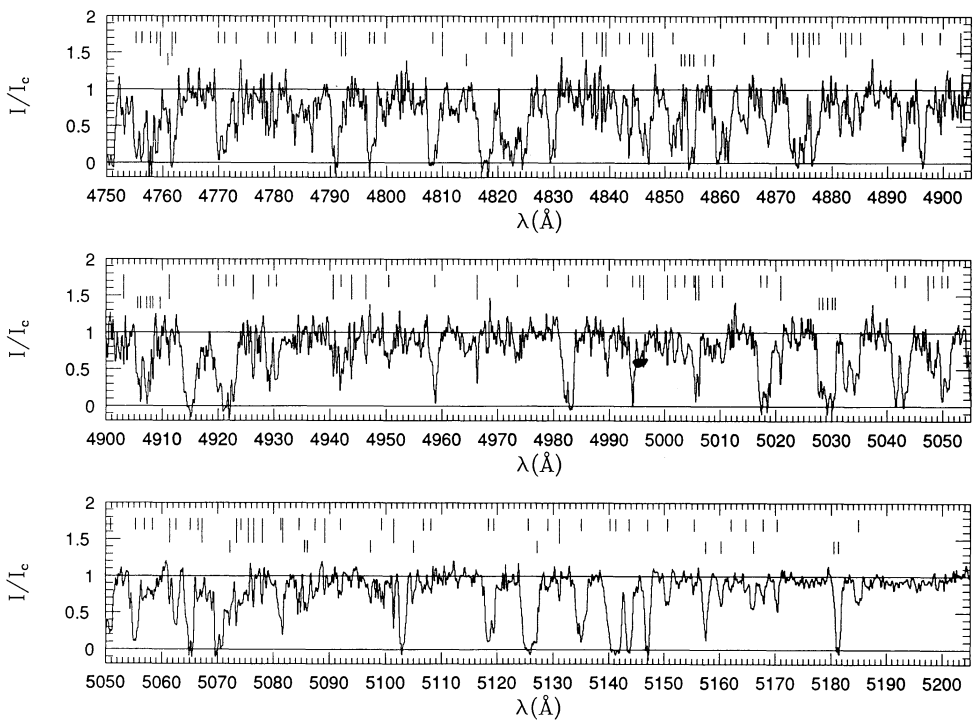

FIG. 1.—Echelle spectrum of PKS 2126−158 in the Lyman-alpha forest normalized to unit continuum. Upper and lower marks show Lyα and heavy element components, respectively, listed in Table 1. The long upper marks indicate Lyα lines with $b \leq 15$ km s^{-1}.

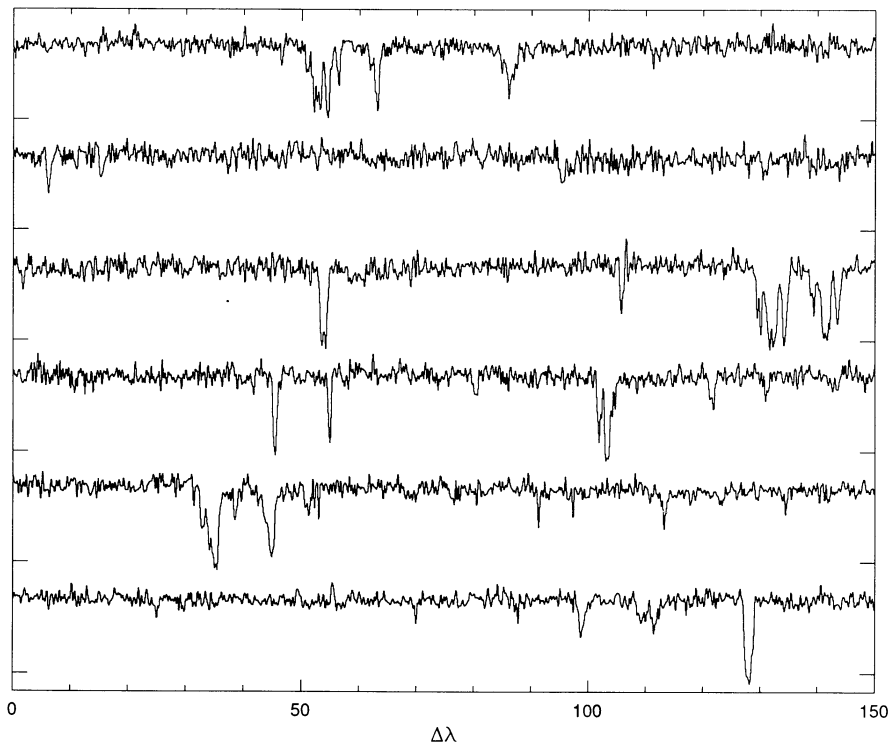

FIG. 2*a*

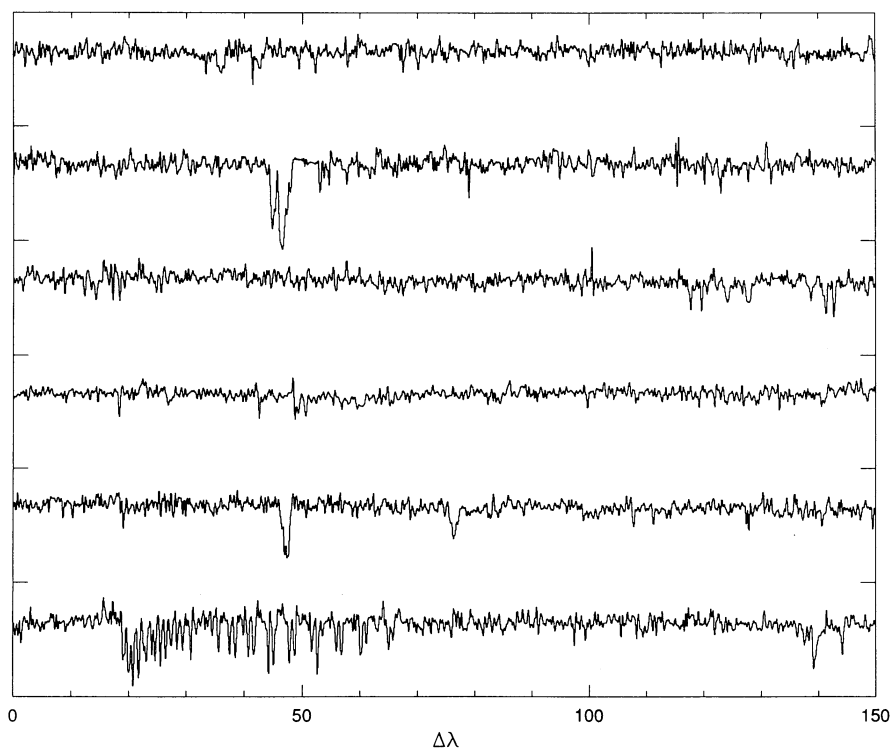

FIG. 2*b*

FIG. 2.—Normalized echelle spectrum of PKS 2126−158 redward of the QSO Lyman-alpha emission (*a*) from 5200 Å (*top left*) to 6100 Å (*lower right*) and (*b*) from 6100 Å to 7000 Å. Ticks on the vertical axis show the zero flux levels and are 1.5 spaced.

the continuum are selected to form a statistically well defined sample.

In general this method can be noiser than the selection based on the equivalent width (EW), which is an integral quantity. However, in high-redshift spectra, where blending is severe, the EW may become a poorly defined quantity, depending on the details of the deblending procedure. A check of the method has been performed considering a 50 Å region redward of the peak of the QSO Lyα emission, indicating that the number of spurious lines due to noise should be $\lesssim 5$ in our Lyα sample. The selection method used here corresponds to a well-defined locus in the b–log $N_{\rm H\,I}$ plane, as shown in the next section.

A χ^2 fitting of Voigt profiles, convolved with the instrumental spread function, was adopted to derive the redshift z, the Doppler parameter $b = 2^{1/2}\sigma$ and the column density N for isolated lines and individual components of blends. The fitting code makes use of the MINUIT package of the CERN library which adopts several methods to find the global minimum. The number of components of each absorption feature is assumed to be the minimum giving a probability of random deviation $P > 0.05$.

In estimating the parameter errors, the correlation between neighboring pixels introduced by data rebinning has been taken into account through a χ^2 renormalization factor estimated by comparison of the noise levels in the raw and final data (see Carswell et al. 1991).

The list of all individual absorption lines is given in Table 1 where lines without identification label ID are assumed to be Lyα absorptions and lines without b and log $N_{\rm H\,I}$ values correspond to situations where the deblending is uncertain.

Heavy element systems have been identified using the list of Morton (1991) and considering the subset of the lines most frequently seen in QSO absorption spectra. Redshift systems have been selected adopting the method of Young et al. (1979) which looks for significant excesses of identifications at all possible redshifts in the wavelength range observed. The identified heavy element systems are listed in Table 2.

Besides the systems previously found at lower resolution (Young et al. 1979; Sargent, Boksenberg, & Steidel 1988), we show a system identified by the C IV doublet, and a low-redshift system identified by a Ca II doublet, whose column densities and equivalent widths were too weak to be detected in previous observations. In three of the seven C IV systems, a complex velocity structure has been revealed, with Δv in the range 65–300 km s^{-1}. These structures are often present in high-resolution spectra (see, e.g., Bechtold, Green, & York 1987). A brief summary for each system is given below:

z = 0.6626.—This system consists of two Ca II doublets, split by 65 km s^{-1}. The values of the column density are in agreement with those observed in galaxies of similar redshift (Blades 1988). Mg II lines are observed but fall outside the range with an acceptable S/N ratio and were not fitted.

z = 2.33126.—This possible system, never observed before, consists of a C IV doublet and two Si II λ1526 lines, all inside Lyα forest. Other transitions from Si II and Si IV lie outside our range with the exception of Si II λ1808 that, with the value of b and N inferred from Si II λ1526, is too weak to be detected.

z = 2.3935.—This is the system formerly suggested by Young et al. and confirmed by Sargent, Steidel, & Boksenberg (1990). With our data these features are clearly resolved and fitted with two distinct components. Furthermore, we identify Si II λ1526 and λ1808. Si II λ1808 has b and N much higher than Si II λ1526, because of blending with other features. Other Si II lines lie outside the observed range. No other element is observed.

z = 2.45959.—This system, identified by Sargent et al. (1988), is defined by the C IV doublet only. Si IV lines, if present, are blended with the stronger C II complex of $z = 2.637$. Si II is not observed.

z = 2.638.—For this system we are able to show a velocity structure of at least seven components, with a spread of 270 km s^{-1} (Fig. 3*a*). The number of components and the relative redshifts have been assessed in the C IV doublet which lies outside the Lyα region and has a good S/N ratio.

Lines falling in the Lyα region are difficult to examine, since they may be blended with H I lines. In these cases (e.g., C II, C II*), we have identified and fitted only components in coincidence—within 0.1 Å—with C IV components. Nevertheless the b and N values of these lines, and even their existence, are to be considered as doubtful.

In addition to the C IV doublet, we have found and fitted C II λ1334, its fine-structure excited level C II λ1335; Al II λ1670; Si IV λλ1393, 1402; Si II λ1526; O I λ1302, all already identified by Young et al., and Al III λλ1854, 1862; Mg I λ1827; and Fe II λ1608. No fine-structure line of Si II has been observed.

z = 2.6787.—This system, identified by Sargent et al. (1988), shows a clear C IV doublet, a Si IV doublet, a possible C II line, and a Fe II λ1608. Si IV doublet has been fitted using Si IV λ1402 only, since Si IV λ1398 is blended with a wide Lyα line. The C II line is not certain, being relatively weak and in a region with poor S/N. Despite an accurate search, no other line from low-ionization elements has been found.

z = 2.72795.—This weak system is identified only by its C IV doublet which falls outside the Lyα forest and does not show any other identified line.

z = 2.768.—This is the third complex system found in this spectrum. It appears as a blended feature of $\Delta v = 150$ km s^{-1}, plus a line at $\Delta v \simeq +230$ km s^{-1} from the center of the main feature. The total width is 300 km s^{-1}.

Five components have been identified using low-ionization lines falling outside the Lyα forest, and all the lines unambiguously identified in the Lyα forest have been fitted. The C IV doublet shows only three components (see Fig. 3*b*). Of the elements identified by Young et al., C II λ1334; Al II λ1670; Si IV λλ1393, 1402; Si II λ1526; O I λ1302 have been fitted, while Si II λ1304, Si II λ1260, and fine-structure excited level C II λ1335 are not considered because of severe line blending and saturation. Weak Al III λ1854 and Fe II λ1608 have been observed, while no fine-structure line of Si II has been observed.

z = 2.8195.—This system was identified by Meyer & York (1987) as a C IV doublet only, at $z = 2.8194$. We identify the low-ionization lines C II λ1334, Si II λ1260, and Al II λ1670, at the slightly higher redshift $z = 2.8196$.

z = 2.9069.—This C IV system (Meyer & York 1987) shows also Al II λ1670 and Si IV λλ1393, 1402.

z = 2.9676.—This is a Lyman-limit system identified by Sargent et al. (1990). The associated Lyα line has a complex structure and the column density of the saturated component is uncertain. The value of log $N_{\rm H\,I} \sim 17$ derived from the Lyman edge requires Doppler parameter values $b \lesssim 10$ km s^{-1}. At high resolution, the C IV identification is doubtful (a wavelength discrepancy of about 0.5 Å is observed between the two components of the doublet) and no other heavy elements have been identified.

TABLE 1

PKS 2126−158 ABSORPTION-LINE PARAMETERS

λ_{vac}	±	b	±	log N	±	ID
4730.32	0.03	11.17	2.73	13.56	0.09	SiIV 1393
4736.65	0.03	9.80	3.03	16.34	0.27	OI 1302
4737.33	0.06	6.30	6.93	14.41	0.09	OI 1302
4737.73	0.08	9.60	8.84	14.24	0.10	OI 1302
4755.19	0.05	22.07	4.69	13.97	0.10	
4756.25	0.08	30.05	6.66	14.01	0.06	
4757.79	0.03	19.23	6.24	14.69	0.70	
4758.90	0.04	17.56	4.21	13.82	0.10	
4759.58	0.08	8.66	7.79	13.17	0.16	
4760.91	0.03	11.17	2.73	13.56	0.09	SiIV 1402
4761.66	0.05	12.59	2.65	14.29	0.39	
4762.29	0.12	17.45	7.96	13.46	0.18	
4769.96	0.05	17.88	3.89	13.88	0.14	
4771.11	0.10	49.18	8.24	14.05	0.06	
4773.15	0.03	21.74	3.12	13.52	0.05	
4778.82	0.08	33.79	7.38	13.56	0.08	
4780.18	0.06	24.28	4.94	13.48	0.09	
4783.72	0.10	47.09	10.00	13.72	0.08	
4786.69	0.04	18.52	4.15	13.62	0.08	
4790.88	0.05	28.09	6.20	14.42	0.25	
4791.95	0.06	12.34	7.54	13.24	0.17	
4792.70	0.06	12.72	8.07	13.10	0.16	
4796.96	0.06	18.30	5.93	14.21	0.27	
4797.81	0.13	25.79	9.39	13.75	0.14	
4799.73	0.21	69.45	22.24	13.63	0.10	
4808.30	0.04	41.59	6.84	14.62	0.20	
4810.01	0.08	12.58	8.36	13.06	0.16	
4814.31	0.05	12.46	10.71	12.48	0.23	SiII 1260
4817.86	0.02	56.55	12.18	14.80	0.28	
4821.15	0.02	44.62	8.88	14.02	0.03	
4822.48	0.09	12.56	4.13	16.93	0.11	
4824.38	0.06	63.16	5.58	14.25	0.04	
4829.67	0.04	38.82	4.17	14.16	0.06	
4835.13	0.08	14.91	8.76	13.11	0.16	
4837.67	0.08	17.07	11.56	13.22	0.17	
4838.67	0.04	5.95	6.88	12.97	0.16	
4839.31	0.06	10.07	7.18	13.01	0.17	
4841.83	0.05	30.28	4.16	13.65	0.05	
4843.61	0.04	22.10	3.70	13.73	0.06	
4845.96	0.08	37.36	8.71	13.88	0.08	
4847.03	0.04	14.72	5.28	14.01	0.27	
4847.76	0.08	11.81	8.10	13.07	0.17	
4851.43	0.08	55.38	7.20	14.04	0.05	
4852.97	0.03	10.90	3.38	13.98	0.13	CII 1334
4853.59	0.05	2.81	6.63	13.37	1.22	CII 1334
4854.47	0.03	11.30	3.38	15.15	0.75	CII 1334
4855.22	0.04	15.80	3.90	14.42	0.17	CII 1334
4857.24	0.03	10.90	3.38	13.27	0.27	CII* 1335
4858.75	0.05	11.30	3.38	13.78	0.13	CII* 1335
4859.50						CII* 1335
4861.00						CII* 1335
4864.25	0.12	56.34	8.74	13.73	0.06	
4868.49	0.05	45.75	4.64	13.86	0.04	
4872.79	0.06	28.95	6.12	13.95	0.08	
4873.76	0.05	12.43	11.57	14.84	2.70	
4874.82	0.00	30.72	4.37	14.02	0.06	
4875.87	0.04	7.59	6.05	12.93	0.17	
4876.62	0.05	29.02	5.80	14.08	0.08	
4877.59	0.16	26.95	11.36	13.47	0.20	
4881.50	0.06	20.62	6.72	13.41	0.09	
4882.47	0.06	5.87	11.06	12.91	0.29	
4883.55	0.08	32.21	6.28	13.59	0.08	
4885.17	0.10	29.11	9.35	13.33	0.12	
4892.90	0.05	31.03	5.65	13.80	0.06	
4896.26	0.03	27.78	2.73	14.23	0.08	
4899.44	0.18	50.68	21.48	13.49	0.13	
4903.12	0.04	6.99	5.32	12.84	0.17	
4905.61	0.25	20.30	16.64	14.43	0.32	OI 1302
4906.13	0.10	10.30	8.19	14.56	0.23	OI 1302
4907.19	0.04	21.60	1.30	14.77	0.08	OI 1302
4907.83	0.03	4.60	1.82	14.71	0.81	OI 1302
4908.32	0.04	6.03	3.77	14.20	0.29	OI 1302
4909.61	0.03	7.36	9.96	13.36	0.20	CII 1334
4911.26	0.05	8.16	7.20	12.85	0.21	
4915.00						SiII 1304
4920.00	0.09	33.29	9.31	13.86	0.10	
4921.41	0.05	16.61	2.83	17.10	1.03	
4922.78	0.08	28.95	6.23	13.91	0.09	
4926.28	0.04	13.32	4.04	13.37	0.09	
4929.10	0.04	27.53	3.04	13.71	0.04	
4930.46	0.06	28.94	6.05	13.63	0.08	
4940.57	0.04	8.03	5.04	13.19	0.14	
494[illegible]4	0.09	55.63	8.01	13.81	0.05	
4943.85	0.04	11.96	3.86	13.23	0.10	
4946.40	0.06	13.69	5.59	13.07	0.13	
4950.[illegible]	0.12	52.10	13.66	13.54	0.09	
4958.70	0.05	37.90	4.35	13.91	0.04	
4966.31	0.03	10.84	2.81	13.22	0.10	
4973.53	0.14	50.09	14.05	13.43	0.09	
4982.62	0.04	41.51	5.46	14.60	0.17	
4989.60	0.05	23.47	4.17	13.39	0.06	
4994.23	0.04	22.55	2.76	13.81	0.06	
4995.50	0.12	26.52	11.83	13.30	0.13	
4996.22	0.06	6.52	11.34	12.94	0.21	
5000.55	0.05	9.41	6.06	12.89	0.17	
5001.91	0.08	24.82	6.54	13.24	0.09	
5003.67	0.00	32.17	6.89	13.36	0.08	
5005.33	0.44	46.90	25.35	13.50	0.31	
5005.62	0.04	9.06	7.92	13.60	0.40	
5006.17	0.04	9.91	3.54	13.33	0.16	
5008.60	0.18	51.05	20.66	13.40	0.13	
5010.40	0.10	35.23	9.02	13.38	0.09	
5017.25	0.06	22.89	4.98	14.11	0.13	
5018.39	0.10	40.76	7.41	14.12	0.06	
5020.84	0.04	13.48	4.73	13.35	0.09	
5027.69	0.03	14.95	1.69	14.20	0.09	CII 1334
5028.32	0.05	12.69	6.59	14.07	0.16	CII 1334
5029.20	0.04	24.64	10.13	14.69	0.14	CII 1334
5030.11	0.06	11.19	7.92	14.74	0.55	CII 1334
5030.58	0.08	6.84	6.07	13.94	0.17	CII 1334
5032.50						CII* 1335
5034.00						CII* 1335
5041.48	0.03	25.82	2.52	13.98	0.06	
5043.19	0.04	40.42	3.56	14.10	0.04	
5047.33	0.05	8.64	6.58	13.08	0.13	
5048.30	0.08	35.14	7.16	13.60	0.06	
5049.84	0.05	18.03	4.09	13.79	0.09	
5050.83	0.06	29.00	5.51	13.80	0.06	
5055.22	0.01	34.67	2.39	14.03	0.03	
5056.85	0.06	30.81	7.66	13.20	0.09	
5058.31	0.22	55.02	7.08	13.33	0.08	
5061.41	0.05	6.99	9.05	12.88	0.17	
5062.51	0.04	27.73	3.84	13.66	0.04	
5065.08	0.04	33.37	3.73	14.29	0.09	
5066.49	0.09	18.78	8.50	13.09	0.14	
5067.20	0.12	14.83	10.88	12.87	0.22	
5070.00						SiIV 1393
5072.13	0.12	20.40	10.13	13.23	0.17	SiIV 1393
5073.34	0.04	8.26	5.62	13.22	0.16	
5074.16	0.17	45.57	17.73	13.50	0.14	
5075.44	0.06	12.27	7.32	12.94	0.13	
5076.41	0.04	8.63	5.63	12.98	0.12	
5077.96	0.05	10.23	4.39	12.87	0.17	
5081.29	0.08	36.90	6.94	13.63	0.08	
5081.63	0.05	5.45	8.27	12.97	0.27	
5084.53	0.08	26.74	5.82	13.33	0.08	
5085.51	0.05	2.23	1.79	13.99	1.46	SiII 1526
5086.03	0.06	21.80	6.76	13.46	0.09	SiII 1526
5087.40	0.10	34.37	8.80	13.18	0.09	
5089.14	0.08	8.39	9.28	12.56	0.31	
5091.88	0.08	23.82	5.86	13.02	0.10	
5097.28	0.09	20.69	12.34	13.59	0.19	CII 1334
5099.25	0.17	62.69	16.48	13.44	0.09	
5101.43	0.03	10.00	2.81	13.20	0.10	
5103.00						SiIV 1402
5104.93	0.12	20.40	10.13	13.23	0.17	SiIV 1402
5106.74	0.17	35.61	19.40	13.01	0.18	
5108.08	0.26	33.33	27.73	12.99	0.31	

TABLE 1—*Continued*

λ_{vac}	±	b	±	log N	±	ID
5118.41	0.04	26.83	3.37	13.99	0.06	
5119.37	0.03	16.25	3.28	13.56	0.08	
5125.53	0.03	47.48	3.33	14.54	0.08	
5127.08	0.06	26.26	6.10	13.41	0.08	SiIV 1393
5129.00	0.05	30.97	4.20	12.95	0.13	
5131.09	0.08	7.93	8.94	12.82	0.20	
5134.98	0.05	52.65	4.78	14.09	0.04	
5140.20	0.57	49.91	19.93	13.87	0.39	
5141.25	0.04	35.77	3.55	15.03	0.22	
5143.64	0.00	29.70	1.95	14.26	0.05	
5146.99	0.03	23.73	2.48	14.16	0.09	
5150.61	0.06	31.57	4.74	13.35	0.06	
5155.42	0.16	25.19	19.33	12.84	0.23	
5157.45	0.01	28.87	2.68	13.97	0.04	CIV 1548
5160.24	0.06	26.26	6.10	13.41	0.08	SiIV 1402
5162.03	0.17	32.15	16.50	12.94	0.17	
5164.66	0.16	22.89	14.34	12.86	0.22	
5166.03	0.01	28.87	2.68	13.97	0.04	CIV 1550
5167.80	0.10	34.33	7.10	13.22	0.08	
5170.31	0.05	22.54	4.09	13.24	0.06	
5180.50	0.13	15.95	10.61	12.93	0.20	SiII 1526
5181.31	0.00	21.42	1.57	14.46	0.10	SiII 1526
5184.94	0.09	42.56	7.57	13.43	0.06	
5250.87	0.10	8.10	12.22	12.85	0.27	SiIV 1393
5251.91	0.22	54.40	17.03	13.58	0.10	SiIV 1393
5252.10	0.04	16.39	5.61	13.59	0.11	SiIV 1393
5252.85	0.07	21.22	11.17	13.37	0.17	SiIV 1393
5253.49	0.06	6.64	5.60	12.70	0.29	SiIV 1393
5256.31	0.04	17.51	4.07	13.01	0.08	SiIV 1393
5262.00	0.08	20.14	5.60	13.58	0.10	CIV 1550
5263.15	0.03	20.84	2.04	14.18	0.04	CIV 1550
5284.84	0.10	8.10	12.22	12.85	0.27	SiIV 1402
5285.89	0.22	54.40	17.03	13.58	0.10	SiIV 1402
5286.08	0.04	16.39	5.61	13.59	0.11	SiIV 1402
5286.82	0.07	21.22	11.17	13.37	0.17	SiIV 1402
5287.47	0.06	6.64	5.60	12.70	0.29	SiIV 1402
5290.31	0.04	17.51	4.07	13.01	0.08	SiIV 1402
5356.12	0.05	23.87	5.17	13.55	0.06	CIV 1548
5365.03	0.05	23.87	5.17	13.55	0.06	CIV 1550
5445.41	0.03	29.71	4.71	13.15	0.05	SiIV 1393
5480.63	0.03	29.71	4.71	13.15	0.05	SiIV 1402
5551.52	0.04	2.09	5.29	12.83	0.35	SiII 1526
5553.56	0.05	16.38	3.29	14.18	0.13	SiII 1526
5554.20	0.01	5.99	1.56	15.22	0.84	SiII 1526
5554.67	0.05	3.16	3.93	12.94	0.35	SiII 1526
5629.45	0.03	9.22	2.98	13.46	0.08	CIV 1548
5630.04	0.00	10.91	2.26	13.80	0.06	CIV 1548
5630.74	0.14	15.64	5.32	13.29	0.09	CIV 1548
5631.73	0.39	24.22	4.30	14.42	0.29	CIV 1548
5632.32	0.39	7.18	4.67	14.61	0.26	CIV 1548
5632.78	0.39	12.24	5.07	13.89	0.22	CIV 1548
5634.21	0.03	23.27	1.73	14.16	0.04	CIV 1548
5638.82	0.03	9.22	2.98	13.46	0.08	CIV 1550
5639.40	0.00	10.91	2.26	13.80	0.06	CIV 1550
5640.10	0.14	15.64	5.32	13.29	0.09	CIV 1550
5641.10	0.39	24.22	4.30	14.42	0.29	CIV 1550
5641.69	0.39	7.18	4.67	14.61	0.26	CIV 1550
5642.15	0.39	12.24	5.07	13.89	0.22	CIV 1550
5643.58	0.03	23.27	1.73	14.16	0.04	CIV 1550
5695.45	0.00	13.91	1.23	14.15	0.06	CIV 1548
5704.93	0.00	13.91	1.23	14.15	0.06	CIV 1550
5751.84	0.01	11.34	2.08	13.67	0.09	SiII 1526
5752.33	0.06	8.78	6.30	13.16	0.14	SiII 1526
5753.35	0.01	15.98	5.41	14.71	0.72	SiII 1526
5754.14	0.04	7.82	5.34	13.19	0.12	SiII 1526
5754.67	0.05	6.03	7.88	13.00	0.14	SiII 1526
5771.59	0.08	28.65	6.14	13.47	0.08	CIV 1548
5781.19	0.08	28.65	6.14	13.47	0.08	CIV 1550
5832.93	0.05	20.27	4.38	13.55	0.08	CIV 1548
5834.12	0.14	23.58	9.19	13.86	0.17	CIV 1548
5835.16	0.06	23.34	3.17	14.47	0.06	CIV 1548
5838.59	0.05	16.64	4.11	13.36	0.09	CIV 1548
5842.64	0.05	20.27	4.38	13.55	0.08	CIV 1550
5843.82	0.14	23.58	9.19	13.86	0.17	CIV 1550
5844.86	0.06	23.34	3.17	14.47	0.06	CIV 1550
5848.30	0.05	16.64	4.11	13.36	0.09	CIV 1550
5850.77	0.14	12.87	11.87	13.50	0.27	FeII 1608
5851.35	0.10	10.43	8.45	13.59	0.22	FeII 1608
5851.84	0.00	1.27	9.26	12.89	0.88	FeII 1608
5913.29	0.03	27.16	5.23	13.53	0.07	CIV 1548
5917.85	0.12	14.39	9.84	13.41	0.20	FeII 1608
5923.12	0.03	27.16	5.23	13.53	0.07	CIV 1550
6048.94	0.03	31.20	3.85	13.64	0.04	CIV 1548
6059.00	0.03	31.20	3.85	13.64	0.04	CIV 1550
6060.01	0.06	11.00	9.84	13.47	0.09	FeII 1608
6060.43	0.07	2.93	4.44	12.96	0.20	FeII 1608
6061.51	0.08	28.00	6.58	14.00	0.08	FeII 1608
6062.42	0.08	3.04	6.14	13.12	0.42	FeII 1608
6077.83	0.05	18.72	3.08	13.55	0.35	AlII 1670
6078.27	0.12	7.32	2.90	13.92	0.36	AlII 1670
6078.78	0.01	2.03	0.88	13.93	1.23	AlII 1670
6135.95	0.13	35.68	10.22	14.92	0.10	SiII 1808
6294.71	0.05	12.16	3.15	12.78	0.09	AlII 1670
6295.23	0.06	6.83	5.39	12.28	0.18	AlII 1670
6296.36	0.00	15.11	1.36	13.75	0.17	AlII 1670
6297.24	0.04	12.32	5.00	12.48	0.10	AlII 1670
6297.86	0.06	5.42	4.21	12.01	0.21	AlII 1670
6381.77	0.05	4.52	4.52	11.74	0.32	AlII 1670
6527.79	0.07	24.59	6.54	12.34	0.09	AlII 1670
6541.31	0.04	11.96	3.74	12.34	0.09	CaII 3934
6542.71	0.04	10.09	2.73	12.35	0.08	CaII 3934
6599.19	0.04	11.96	3.74	12.34	0.09	CaII 3969
6600.60	0.04	10.09	2.73	12.35	0.08	CaII 3969
6649.67	0.06	2.35	5.88	13.46	0.90	MgI 1827
6746.38	0.03	7.90	7.20	12.32	0.40	AlIII 1854
6746.96	0.13	12.49	9.23	12.93	0.22	AlIII 1854
6747.53	0.01	13.20	3.12	12.93	0.14	AlIII 1854
6775.74	0.03	7.90	7.20	12.32	0.40	AlIII 1862
6776.32	0.13	12.49	9.23	12.93	0.22	AlIII 1862
6776.90	0.01	13.20	3.12	12.93	0.14	AlIII 1862
6989.35	0.06	23.47	4.89	13.07	0.06	AlIII 1854

4. THE LYMAN-ALPHA SAMPLE

4.1. *Line Statistics*

After removing metal line and Lyman-limit systems, a complete sample of Lyα lines in the region from 4750 to 5200 Å can be obtained from Table 1. Its distribution in the b–log $N_{\rm H\,I}$ plane is shown in Figure 4.

Two curves of constant central line flux, containing most of the sample, are also shown. The upper envelope represents our selection criterion: only lines with central flux less than the threshold are included in the complete sample. The lower curve corresponds to a central flux of 0.1 where the noise level is comparable to the signal and where lines start to saturate. Thus, the unsaturated subsample of the selected lines would show a tight correlation.

This by no means implies that the b–$N_{\rm H\,I}$ correlation found by Pettini et al. (1990) is entirely artificial. In fact, considering all the Lyα sample, the saturated lines are not uniformly dis-

TABLE 2

HEAVY ELEMENT ABSORPTION SYSTEMS

λ_{vac}	ID		z	±	b	±	log N.	±
			$z = 0.6626$					
6541.31	CaII 3934	a	0.662435	.000010	11.96	3.74	12.34	.09
6599.19	CaII 3969							
6542.71	CaII 3934	b	0.662790	.000009	10.09	2.73	12.35	.08
6600.60	CaII 3969							
			$z = 2.33126$					
5157.45	CIV 1548		2.331267	.000007	28.87	2.68	13.97	.04
5166.03	CIV 1550							
5085.51	SiII 1526	a	2.331033	.000030	2.23	1.79	13.99	1.46
5086.03	SiII 1526	b	2.331373	.000045	21.80	6.76	13.46	.09
			$z = 2.3935$					
5253.26	CIV 1548	a	2.393151	.000048	20.14	5.60	13.58	.10
5262.00	CIV 1550							
5254.41	CIV 1548	b	2.393894	.000016	20.84	2.08	14.18	.04
5263.15	CIV 1550							
5180.50	SiII 1526	a	2.393252	.000082	15.95	10.61	12.93	.20
5181.31	SiII 1526	b	2.393783	.000001	21.42	1.57	14.46	.10
6135.95	SiII 1808	b	2.393754	.000073	35.68	10.22	14.92	.10
4730.32	SiIV 1393	b	2.393939	.000019	11.17	2.73	13.56	.09
4760.91	SiIV 1402							
			$z = 2.45959$					
5356.12	CIV 1548	a	2.459590	.000036	23.87	5.17	13.55	.06
5365.03	CIV 1550							
			$z = 2.638$					
5629.45	CIV 1548	a	2.636138	.000019	9.22	2.98	13.46	.08
5638.82	CIV 1550							
5630.04	CIV 1548	b	2.636519	.000001	10.91	2.26	13.80	.06
5639.40	CIV 1550							
5630.74	CIV 1548	c	2.636971	.000088	15.64	5.32	13.29	.09
5640.10	CIV 1550							
5631.73	CIV 1548	d	2.637610	.000252	24.22	4.31	14.42	.29
5641.10	CIV 1550							
5632.32	CIV 1548	e	2.637991	.000252	7.18	4.67	14.61	.26
5641.69	CIV 1550							
5632.78	CIV 1548	f	2.638288	.000252	12.24	5.07	13.89	.22
5642.15	CIV 1550							
5634.21	CIV 1548	g	2.639212	.000016	23.27	1.73	14.16	.04
5643.58	CIV 1550							
4852.97	CII 1334	b	2.636465	.000021	10.90	3.38	13.98	.13
4853.59	CII 1334	c	2.636922	.000016	2.81	6.63	13.37	1.22
4854.47	CII 1334	d	2.637611	.000021	11.30	3.38	15.15	.75
4855.22	CII 1334	ef	2.638159	.000022	15.80	3.90	14.42	.17
4857.11	CII* 1335	b	2.636357	.000053	10.90	3.38	13.27	.27
4858.75	CII* 1335	d	2.637533	.000034	11.30	3.38	13.78	.13
6077.83	AlII 1670	d	2.637704	.000018	18.72	3.08	13.55	.35
6078.27	AlII 1670	e	2.637967	.000010	7.32	2.90	13.92	.36
6078.78	AlII 1670	f	2.638273	.000005	2.03	0.88	13.93	1.23
6746.38	AlIII 1854	d	2.637413	.000023	7.90	7.20	12.32	.04
6775.74	AlIII 1862							
6746.96	AlIII 1854	e	2.637731	.000002	12.49	9.23	12.93	.22
6776.32	AlIII 1862							
6747.53	AlIII 1854	f	2.638038	.000006	13.20	3.12	12.93	.14
6776.90	AlIII 1862							
5072.13	SiIV 1393	g	2.639183	.000087	20.40	10.13	13.23	.17
5104.93	SiIV 1402							
5551.52	SiII 1526	a	2.636272	.000023	2.09	5.29	12.83	.35
5553.56	SiII 1526	d	2.637608	.000031	16.38	3.29	14.18	.13
5554.20	SiII 1526	e	2.638027	.000005	5.99	1.56	15.22	.84
5554.67	SiII 1526	f	2.638335	.000032	3.16	3.93	12.94	.35
6649.67	MgI 1827	def	2.637804	.000035	2.35	5.88	13.46	.90
4736.65	OI 1302	d	2.637509	.000001	9.80	3.03	16.34	.27
4737.33	OI 1302	e	2.638047	.000001	6.30	6.93	14.41	.09
4737.73	OI 1302	f	2.638339	.000003	9.60	8.84	14.24	.10
5850.77	FeII 1608	d	2.637518	.000088	12.87	11.87	13.50	.27
5851.35	FeII 1608	e	2.637879	.000061	10.43	8.45	13.59	.22
5851.84	FeII 1608	f	2.638183	.000004	1.27	9.26	12.89	.88
			$z = 2.6787$					
5695.45	CIV 1548	a	2.678768	.000004	13.91	1.23	14.15	.06
5704.93	CIV 1550							
5127.08	SiIV 1393	a	2.678609	.000051	26.26	6.10	13.41	.08
5160.24	SiIV 1402							
4909.61	CII 1334	a	2.678899	.000021	7.36	9.96	13.36	.20
5917.85	FeII 1608	a	2.679223	.000070	14.39	9.84	13.41	.20
			$z = 2.72795$					
5771.59	CIV 1548	a	2.727948	.000052	28.65	6.14	13.47	.08
5781.19	CIV 1550							
			$z = 2.768$					
5832.93	CIV 1548	a	2.767568	.000036	20.27	4.38	13.55	.08
5842.64	CIV 1550							
5834.12	CIV 1548	c	2.768337	.000094	23.58	9.19	13.86	.17
5843.82	CIV 1550							
5835.16	CIV 1548	d	2.769009	.000040	23.34	3.17	14.47	.06
5844.86	CIV 1550							
5838.59	CIV 1548	f	2.771224	.000036	16.64	4.11	13.36	.09
5848.30	CIV 1550							
6294.71	AlII 1670	a	2.767511	.000032	12.16	3.15	12.78	.09
6295.23	AlII 1670	b	2.767822	.000044	6.83	5.39	12.28	.18
6296.36	AlII 1670	c	2.768499	.000001	15.11	1.36	13.75	.17
6297.24	AlII 1670	d	2.769014	.000022	12.32	5.00	12.48	.10
6297.86	AlII 1670	e	2.769391	.000036	5.42	4.21	12.01	.21
5751.84	SiII 1526	a	2.767482	.000010	11.34	2.08	13.67	.09
5752.33	SiII 1526	b	2.767803	.000044	8.78	6.30	13.16	.14
5753.35	SiII 1526	c	2.768452	.000003	15.98	5.41	14.71	.72
5754.14	SiII 1526	d	2.768989	.000029	7.82	5.34	13.19	.12
5754.67	SiII 1526	e	2.769336	.000031	6.03	7.88	13.00	.14
5027.69	CII 1334	a	2.767380	.000023	14.95	1.69	14.20	.09
5028.32	CII 1334	b	2.767852	.000038	12.69	6.59	14.07	.16
5029.20	CII 1334	c	2.768511	.000027	24.64	10.13	14.69	.14
5030.11	CII 1334	d	2.769193	.000045	11.19	7.92	14.74	.55
5030.58	CII 1334	e	2.769545	.000057	6.84	6.07	13.94	.17
4905.61	OI 1302	a	2.767416	.000088	20.30	16.64	14.43	.32
4906.13	OI 1302	b	2.767677	.000021	10.30	8.19	14.56	.23
4907.19	OI 1302	c	2.768476	.000027	21.60	1.30	14.77	.08
4907.83	OI 1302	d	2.768959	.000007	4.60	1.82	14.71	.81
4908.32	OI 1302	e	2.769343	.000034	6.03	3.77	14.20	.29

TABLE 2—*Continued*

λ_{vac}	ID		z	±	b	±	log N	±
5250.87	SiIV 1393	a	2.767413	.000044	8.10	12.22	12.85	.27
5284.84	SiIV 1402							
5251.91	SiIV 1393	b	2.768173	.000173	54.40	17.03	13.58	.10
5285.89	SiIV 1402							
5252.10	SiIV 1393	c	2.768309	.000029	16.39	5.61	13.59	.11
5286.08	SiIV 1402							
5252.85	SiIV 1393	d	2.768847	.000053	21.22	11.17	13.37	.17
5286.82	SiIV 1402							
5253.49	SiIV 1393	e	2.769306	.000046	6.60	5.60	12.70	.29
5287.47	SiIV 1402							
5256.31	SiIV 1393	f	2.771330	.000031	17.51	4.07	13.01	.08
5290.31	SiIV 1402							
6989.35	AlIII 1854	c	2.768420	.000032	23.47	4.89	13.07	.06
6060.01	FeII 1608	a	2.767606	.000037	11.00	9.84	13.47	.09
6060.43	FeII 1608	b	2.767867	.000043	2.93	4.44	12.96	.20
6061.51	FeII 1608	c	2.768538	.000049	28.00	6.58	14.00	.08
6062.42	FeII 1608	e	2.769104	.000047	3.04	6.14	13.12	.42
			$z = 2.8195$					
5913.29	CIV 1548		2.819474	.000033	27.16	5.23	13.53	.07
5923.12	CIV 1550							
5097.28	CII 1334		2.819526	.000071	20.69	12.34	13.59	.19
4814.31	SiII 1260		2.819601	.000060	12.46	10.71	12.48	.23
6381.77	AlII 1670		2.819619	.000029	4.52	4.52	11.74	.32
			$z = 2.9069$					
6048.94	CIV 1548		2.9070792	.000019	31.20	3.85	13.64	.04
6059.00	CIV 1550							
6527.79	AlII 1670		2.9070314	.000041	24.59	6.54	12.34	.09
5445.41	SiIV 1393		2.9069926	.000021	29.71	4.71	13.15	.05
5480.63	SiIV 1402							

tributed in the same range of b occupied by unsaturated lines. In particular, isolated lines with $b < 20$ and log $N_{\rm H\,I} > 13.5$ are not present in our spectrum. Thus either they are really absent, or they are systematically hidden in blends.

A careful inspection of all the saturated lines with log $N_{\rm H\,I} \gtrsim 14.5$ suggests that most of them could be unresolved blends. The components could occupy the region $b \gtrsim 30$ and log $N_{\rm H\,I} \lesssim 14$ as can be seen, for example, in Figure 1 of Giallongo et al. (1992a), where a simulated blend of lines with log $N_{\rm H\,I} \sim 14$ and with S/N = 6 has been fitted as a single line of $b = 35$ and log $N_{\rm H\,I} = 15.1$, comparable with the line of highest column density in our sample.

Even in the absence of an intrinsic b–$N_{\rm H\,I}$ correlation, the fraction of lines with $b < 20$ would be an important information on the physical structure of the clouds. In our Lyα sample, 47 lines, i.e., $\simeq 36\%$, have $b < 20$, and 29 lines, i.e., 22% have $10 \leq b \leq 20$, independently of their column densities. The fraction of narrow lines is higher than the one found by Rauch et al. (1992) even neglecting those with $b < 10$ which could be spurious or unidentified metal lines.

However, it is not possible to derive the intrinsic fraction of narrow lines because of the selection bias against the broad-weak lines and the intrinsic absence of narrow-strong lines. For example, restricting our sample to lines with $13.3 \leq \log N_{\rm H\,I} \leq 13.6$, the fraction of lines with $10 \leq b \leq 20$ reduces to 14%.

The presence of a substantial number of narrow Lyα lines, together with the trend for high column densities to be associated with large b values, could be explained by the gravitationally confined cloud models of Petitjean et al. (1993).

The column density distribution of the Lyα lines is shown in Figure 5. For values log $N_{\rm H\,I} \lesssim 13.3$ a selection bias is expected since (see Fig. 4) only the narrower lines are included in the sample. This is confirmed by the drop of the column density distribution below log $N_{\rm H\,I} = 13$. A value log $N_{\rm H\,I} = 13.3$ has been adopted as completness limit of the sample.

Performing a maximum likelihood analysis of the $N_{\rm H\,I}$ distribution in the redshift range $z = 2.911$–3.166, with the usual assumption of a power-law shape $N_{\rm H\,I}^{-\beta}$, a value $\beta = 1.76$ is found, consistent with the values reported by similar previous analyses (see, e.g., Rauch et al. 1992).

However, a systematic trend seems to be present in the estimate of the power-law index: lower β values are obtained when high column density lines are excluded from the analysis, as shown in Table 3. It is sufficient to remove few lines from the sample to reduce the power-law index from 1.76 to 1.5–1.6. If lines with log $N_{\rm H\,I} \gtrsim 14.5$ are systematically unresolved blends in our spectrum, then this flatter slope is a better representation of the intrinsic column density distribution of the optically thin Lyα lines.

To check the reliability of this new estimate, we have looked for a similar trend in other high resolution samples available in the literature. Q0420−388 (Atwood, Baldwin, & Carswell 1985) and PKS 2000−330 (Carswell et al. 1987) have completeness limits of log $N_{\rm H\,I} = 14$ and log $N_{\rm H\,I} = 13.75$, respectively, too close to the adopted upper limit of log $N_{\rm H\,I} = 14.8$ to allow a reliable estimate of the power-law index β. Thus the comparision has been limited to Q0014+813 (Rauch et al. 1992) in the redshift range $z = 2.695$–3.301 and Q1101−264

TABLE 3

MAXIMUM LIKELIHOOD ANALYSIS REMOVING LINES WITHIN 8 Mpc OF THE QSOs

QSO Sample	log N Range	Number of Lines	γ	β	$P(\beta)$
0014−264	13.3–14.8	162	...	1.51 ± 0.10	0.95
1101−264	13.3–14.8	37	...	1.54 ± 0.18	0.98
2126−158	≥13.3	71	...	1.76 ± 0.08	0.43
	13.3–14.8	68	...	1.63 ± 0.13	0.76
1101−264, 2126−158, 0014+813	≥13.3	285	2.14 ± 0.09	1.74 ± 0.01	0.02
	13.3–14.8	275	2.21 ± 0.05	1.53 ± 0.02	0.70
	13.3–13.78	134	2.53 ± 0.52	1.52 ± 0.11	0.99
	13.78–16	150	1.83 ± 0.17	2.03 ± 0.03	0.28

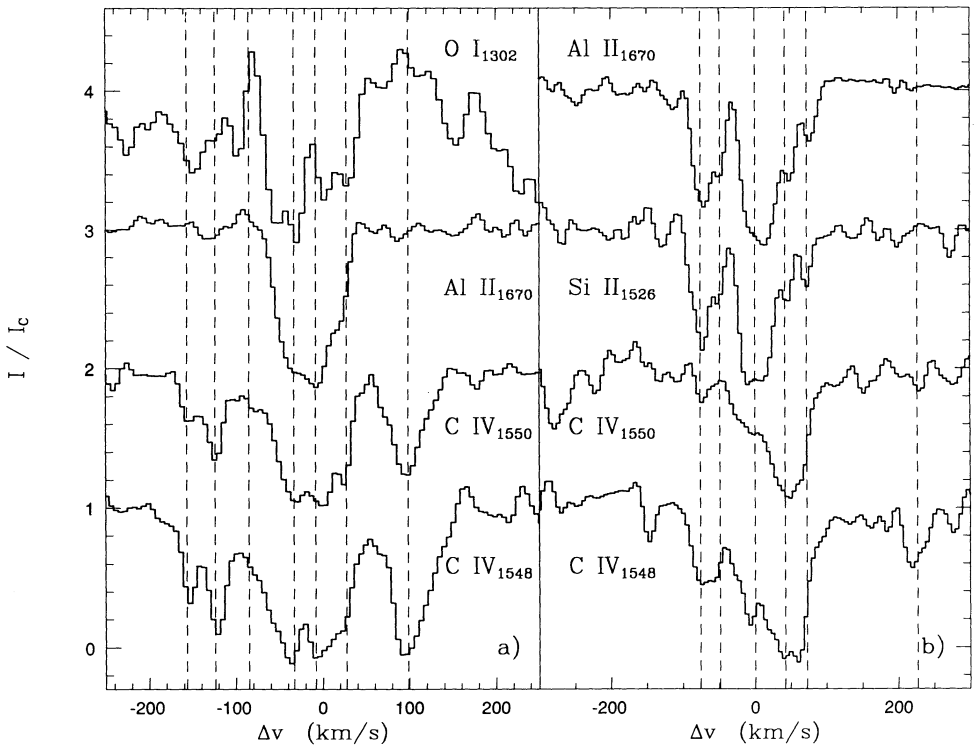

FIG. 3.—The velocity structure of the heavy element systems at (*a*) $z = 2.638$ and (*b*) $z = 2.768$

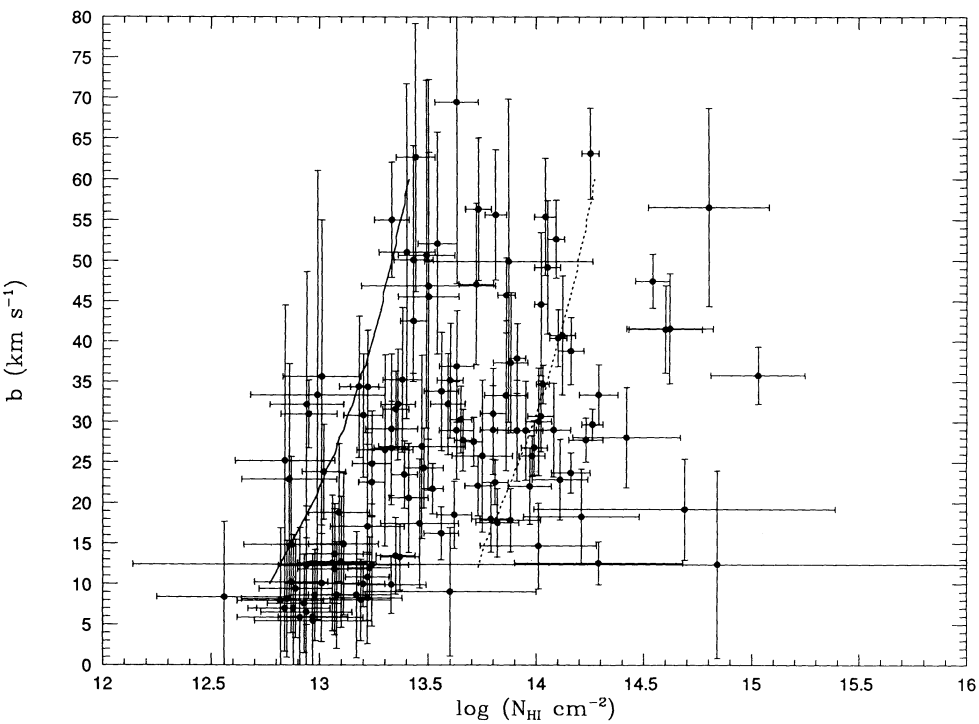

FIG. 4.—Plot of the Doppler parameter b vs. log $N_{\rm H\,I}$ for the Lyα lines listed in Table 1. The continuous curve represents the average selection threshold $I/I_c \simeq 0.7$, and the dashed line represents a central relative intensity of the line equal to 0.1.

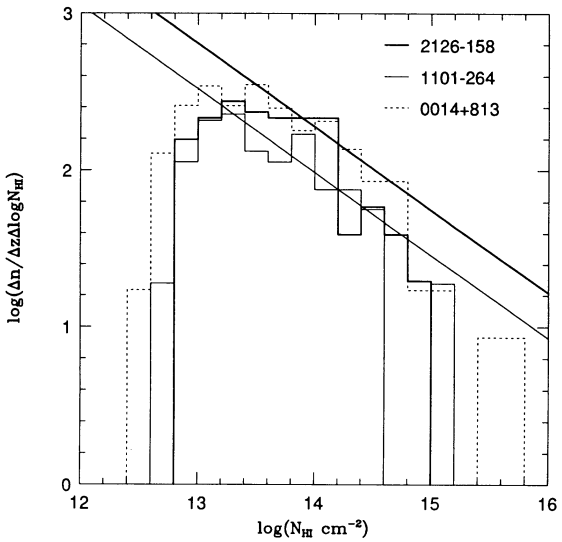

FIG. 5.—Lyα line distribution per unit column density and redshift. The straight lines represent the fit of Table 3 with $\beta = 1.53$ and $\gamma = 2.21$ computed at the average absorption redshifts $z = 2$ of Q1101−264 (*thin line*) and $z = 3$ of PKS 2126−158 (*thick line*).

(Carswell et al. 1991) in the range $z = 1.840$–2.105, which have better resolution and a completeness limit comparable with the value $\log N_{\rm H\,I} = 13.3$ The column density distributions of the individual QSOs are shown in Figure 5.

The results of the maximum likelihood analysis are shown in Table 3 where the line distribution per unit column density evolves according to

$$\rho \equiv \frac{\partial^2 n}{\partial z\, \partial N_{\rm H\,I}} \propto (1+z)^{\gamma} N_{\rm H\,I}^{-\beta} \qquad (1)$$

with β independent of redshift. Considering all the lines with $\log N_{\rm H\,I} \geq 13.3$ and excluding the region affected by the proximity effect ($8h_{100}$ Mpc; see Bajtlik, Duncan, & Ostriker 1988; Lu et al. 1991), the best-fit values are $\gamma = 2.14$ and $\beta = 1.74$, but the single power-law column density distribution is only marginally accepted with a Kolmogorov probability $P(\beta) = 0.02$. Excluding lines with $\log N_{\rm H\,I} > 14.8$ (10 lines), the best-fit value becomes $\gamma = 2.21$ and $\beta = 1.53$ with an acceptance probability $P(\beta) = 0.72$ for the $N_{\rm H\,I}$ distribution. Further lowering the upper limit in column density to values < 14.8 does not change appreciably the value of β. Note that the power-law distribution in $(1 + z)$ is always accepted with high probability.

Both the above estimates of β should be corrected for the line-blanketing effect since high column density lines can conceal several low-$N_{\rm H\,I}$ lines. However, evaluating the effective redshift interval available for lines with $\log N_{\rm H\,I} \simeq 13.3$, we estimate that the observed slope should be increased by less than 0.1, for 0014+813 and 2126−158, and 0.04 for the lower redshift quasar 1101−264.

It is to note that a steeper value $\beta \sim 2$ is found considering lines in the sample with $13.3 \leq \log N_{\rm H\,I} \leq 14.8$ and $b \leq 20$ km s^{-1}. This trend confirms the deficit in the overall sample of strong lines with low b values.

The value of γ is lower than previous estimates obtained from intermediate-resolution samples ($\gamma = 2.75$; Lu et al. 1991). Although our value is based on a relatively small sample, it is worth noting that it is not inconsistent with the value found by Lu et al. since blending effects, present at intermediate resolution, give a systematically higher value of γ connected with the apparent faster evolution of stronger lines, as shown by Trèvese et al. (1992). The absence of such a trend in the present high-resolution sample confirms this interpretation. In fact, stronger lines appear to evolve slower (see Table 3), as pointed out by Giallongo (1991) on the basis of a partly independent equivalent width sample.

The intrinsic distribution appears flatter than previously found in the range $13.3 \leq \log N_{\rm H\,I} \lesssim 15$. There are only 10 lines with $\log N_{\rm H\,I} > 15$ but, since they may be blended, the real number may even be zero. In any case, the best-fit slope beyond the break $\log N_{\rm H\,I} = 15$ is $\beta \sim 2$, a value consistent with the estimate of Petitjean et al. (1992) at slightly lower resolution.

Specific features in the intrinsic column density distribution could have relevant consequences on the estimate of the general ionizing UV flux (see § 5) and the physical properties of the clouds. In fact at $N_{\rm H\,I} \gtrsim 10^{15}$ cm^{-2}, gravitation is expected to control the dynamics of gas in clouds with nonbaryonic dark matter and to generate a signature in the $N_{\rm H\,I}$ distribution (Duncan et al. 1991; Rees 1992).

Barcons & Webb (1991) have pointed out that simulated spectra of randomly distributed lines show significant discrepancy between the observed equivalent width distribution of the Lyα lines in intermediate-resolution QSO spectra and that expected from the steep column density distribution ($\beta = 1.7$) found in high-resolution spectra.

They suggest a model where Lyα clouds are weakly clustered to provide a good fit to the observed equivalent width distribution. However, they have also shown that the discrepancy would disappear with a flatter intrinsic distribution ($\beta \lesssim 1.5$). Thus, our estimate of β indicates that the equivalent width and column density distributions may be consistent even without appreciable clustering. Clustering effects could be present only for the few strong Lyα lines associated with metals.

4.2. *The Average Evolution of Individual Clouds*

The statistical properties of the cloud distribution can be related in a simple way to the average evolution of individual clouds if the cloud distribution $\rho(z, N_{\rm H\,I})$ can be factorized in respect to $N_{\rm H\,I}$ and z, as assumed in equation (1). In a phenomenological, model-independent representation of the evolution, two extreme cases can be considered:

1. A pure number density evolution, where the number in each column density bin changes at a rate proportional to the population of the bin. In a $\log N_{\rm H\,I}$–$\log \rho$ plane, this corresponds to a vertical shift of the column density distribution along the $\log \rho$ axis resulting from a balance of births and deaths of clouds as detectable entities along the line of sight.
2. A pure column density evolution (PCDE), where the column density of each cloud evolves in cosmic time and the number of clouds $[\rho(z, N_{\rm H\,I}(z)]dN_{\rm H\,I}(z)$ is conserved along the evolutionary $N_{\rm H\,I}(z)$ path, resulting in a horizontal shift of the column density distribution along the $\log N_{\rm H\,I}$ axis.

A proper combination of the two cases can be deduced from the evolution of specific features (e.g., break, cutoff) of the observed column density distribution giving quantitative constraints for any specific theoretical models. This is not possible in the case of a featureless power-law distribution unless theoretical constraints are assumed.

For instance, assuming a PCDE of individual clouds of the type $N_{\rm H\,I} = N_{\rm H\,I_0}(1 + z)^k$, the number density of clouds along

the line of sight is

$$\rho(z, N_{\rm H\,I}) = \rho_0(z_0, N_{\rm H\,I_0}) \frac{dN_{\rm H\,I_0}}{dN_{\rm H\,I}} \propto N_{\rm H\,I_0}^{-\beta}(1+z)^{-k}$$
$$\propto N_{\rm H\,I}^{-\beta}(1+z)^{k(\beta-1)} . \quad (2)$$

Thus a column density evolution of this type could be interpreted as a number density with $\gamma = k(\beta - 1)$ (see eq. [1]). Given a specific value of k from a cloud model and values of β and γ derived from the observations, this equality is not necessarily satisfied and a multiplicative source term of the type $\rho' \propto (1+z)^{\gamma'}$ has to be introduced into equation (2), where γ' is related to the time scale of the change in the number of clouds along the line of sight

$$\tau = \frac{\rho'}{\dot{\rho}'} = \frac{1+z}{\gamma'|\dot{z}|} = \frac{1}{\gamma' H_0 (1+z)\sqrt{1+2q_0 z}} . \quad (3)$$

For $q_0 = 0.5$, the time scale is simply proportional to the Hubble time $\tau = 3/(2\gamma')t_{\rm H}$.

For comparison with physical cloud models, it is convenient to relate the cloud number per unit redshift and column density $\rho = \partial^2 n/\partial z\, \partial N_{\rm H\,I}$ to the cloud density per unit comoving volume ϕ (Peterson 1978; Sargent et al. 1980); in fact the number n of clouds intercepted along the line sight dl and with a column density between $N_{\rm H\,I}$ and $N_{\rm H\,I} + dN_{\rm H\,I}$ is

$$dn = \sigma_{N_{\rm H\,I}} \phi (1+z)^3\, dl\, dN_{\rm H\,I} \quad (4)$$

where $\sigma_{N_{\rm H\,I}} = S(z) N_{\rm H\,I}^{-\beta}$ is the cloud cross section per unit column density and ϕ is the comoving volume density. The proper length along the line of sight is

$$\frac{dl}{dz} = \frac{c}{(1+z)H(z)} = \frac{c}{H_0(1+z)^2(1+2q_0 z)^{1/2}} ; \quad (5)$$

then the cloud number per unit redshift and $N_{\rm H\,I}$ is

$$\rho(z, N_{\rm H\,I}) = \frac{c}{H_0} \sigma_{N_{\rm H\,I}} \phi \frac{(1+z)}{(1+2q_0 z)^{1/2}} . \quad (6)$$

In this expression the evolutionary properties of individual clouds are included in $\sigma(z, N_{\rm H\,I})$ and $N_{\rm H\,I}(z)$. Suppose that the column densities of individual clouds evolve in redshift as $N_{\rm H\,I} = N_{\rm H\,I_0}(1+z)^k$. Let us assume for simplicity that to each cloud is associated a single value of the column density $N_{\rm H\,I} = Rn_{\rm H\,I}$, where R and $n_{\rm H\,I}$ are the size and neutral hydrogen volume density, respectively. In this case the cross section can be described by the fraction of clouds per unit column density $f(z, N_{\rm H\,I})$, assumed to have a power-law dependence in $N_{\rm H\,I}$, times the geometrical cross section S of each cloud. If the number of clouds would be conserved then $f dN_{\rm H\,I} = \text{const}$ giving

$$\sigma(z, N_{\rm H\,I}) = S(z, N_{\rm H\,I}) N_{\rm H\,I}^{-\beta'}(1+z)^{k(\beta'-1)} , \quad (7)$$

while possible variation of the cloud number per unit comoving volume is represented in equation (6) as for example $\phi = \phi_0(1+z)^{\gamma'}$.

At variance with Ikeuchi & Turner (1991), this analysis allows for the cosmological evolution of the cloud number per comoving volume. Their purpose was to explore the evolution of the ionizing flux at low redshift, under the implicit assumption of constant comoving number density of clouds. On the contrary, we estimate the evolutionary parameter γ' of the cloud number density at high redshift, for a given evolution of J.

In the range $13.3 \lesssim \log N_{\rm H\,I} \lesssim 15$ where $b \gtrsim 20$, the clouds can be represented by simple pressure confined, isothermal models in ionization equilibrium (Ikeuchi & Ostriker 1986), for which $N_{\rm H\,I} \propto J^{-1} P_{\rm IGM}^{5/3} T_c^{-29/12}$ and $S \propto R^2(z, N_{\rm H\,I}) \propto N_{\rm H\,I}^2/n_{\rm H\,I}^2 \propto N_{\rm H\,I}^2 P_{\rm IGM}^{-4} J^2 T_c^{11/2} \propto (1+z)^s$, where the intergalactic confining medium is assumed in adiabatic expansion with a pressure $P_{\rm IGM} \propto (1+z)^p$ with $p = 5$ and $J \propto (1+z)^j$ is the evolution of an ultraviolet background flux dominated by the quasar contribution. In the interval $z = 2$–4, Madau (1992) estimates $j \simeq -0.6$. Then for $q_0 = 0.5$, equation (6) becomes

$$\rho(z, N_{\rm H\,I}) \propto (1+z)^{\gamma} N_{\rm H\,I}^{-\beta} \propto N_{\rm H\,I}^{-(\beta'-2)}(1+z)^{s+k(\beta'-1)+1/2+\gamma'} , \quad (8)$$

where $\beta = \beta' - 2$, $k = -j + (5/3)p \simeq 8.9$ and $s = -4p + 2j \simeq -21.2$, then $\gamma' \simeq 0.4$ and $\phi \propto (1+z)^{0.4}$. Assuming $q_0 = 0.5$ and $j \simeq -0.6$ the time scale associated to changes of ϕ is $\tau = \phi/\dot{\phi} = 4t_H$ for pressure-confined clouds, implying that the observed evolution along the line of sight is almost entirely due to the evolution of individual expanding clouds.

For comparison, extrapolating to $z = 3$ the value $j = 3$, found by Madau (1992) for $z < 2$, then γ' would raise to 2.2 and τ would fall to $0.7t_H$, indicating a sensible decrease in cosmic time of the number of structures detectable as absorbing clouds.

In any case, if the mass of each cloud is conserved, then $f_N dN_{\rm H\,I} = g_M dM = \text{const}$, and for a power-law distribution $g_M \propto M^{-\delta}$ a value $\delta = (\beta' + 2)/3 \simeq 1.8$ is found.

5. THE PROXIMITY EFFECT

The proximity effect consists in a reduction of the line density in the region affected by the quasar ionizing flux, and it is usually evaluated under the simplifying assumption of a single featureless power-law $N_{\rm H\,I}$ distribution. In the following, this assumption has been relaxed to allow for features like a break or cutoff in the $N_{\rm H\,I}$ distribution.

When the factorization $\rho = (1+z)^{\gamma} f(N_{\rm H\,I})$ is possible, it is convenient to define the coevolving redshift interval $dX_\gamma = (1+z)^{\gamma} dz$. This allows the comparison of the $N_{\rm H\,I}$ distributions $\partial^2 n/\partial X_\gamma\, \partial N_{\rm H\,I} = f(N_{\rm H\,I})$ independently of redshifts.

If the clouds are highly ionized by the UV background and optically thin, the neutral hydrogen column density N of a cloud near a quasar is (the subscript H I is omitted for simplicity):

$$N = \frac{N_\infty}{1+\omega} , \quad (9)$$

where N_∞ is the *intrinsic* column density the same cloud would have at infinite distance from the quasar and $\omega(z, z_Q) = F_\nu/4\pi J$ is the ratio between the Lyman-limit QSO flux impinging on the cloud and the background flux $4\pi J$ at the same frequency (see Bajtlik et al. 1988).

Approaching the quasar, the column density distribution $f(N, \omega)$ changes according to the conservation law $f(N)dN = f(N_\infty)dN_\infty$, namely:

$$f(N, \omega) = f(N_\infty)(1+\omega) . \quad (10)$$

Assuming a power-law distribution in a given interval ($N_{\rm min}$, $N_{\rm max}$), then $f(N) = AN_\infty^{-\beta}(1+\omega) = AN^{-\beta}(1+\omega)^{1-\beta}$, where A

is the normalization constant, and the number of lines in the coevolving redshift interval with a given ω is

$$\frac{\partial n}{\partial X_\gamma}(\omega) = A(N_{\rm max}^{1-\beta} - N_{\rm min}^{1-\beta})\frac{(1+\omega)^{1-\beta}}{1-\beta}, \quad (11)$$

which allows us to explore the possible dependence of the proximity effect on the *intrinsic* column density. The lower limit $N_{\rm min}$ can be fixed in correspondence to the selection threshold adopted to ensure a reasonable completeness of the line sample. In the case of a featureless power law, considering all the lines above the threshold, the last equation reduces to $\partial n/\partial X_\gamma = AN_{\rm min}^{1-\beta}(1+\omega)^{1-\beta}/(\beta-1)$ (see Bajtlik et al. 1988). If an upper cutoff $N_{\infty,\rm max}$ is present in the *intrinsic* distribution, then $N_{\rm max}(\omega) = N_{\infty,\rm max}/(1+\omega)$ and

$$\frac{\partial n}{\partial X_\gamma}(\omega) = A\frac{N_{\infty,\rm max}^{1-\beta} - N_{\rm min}^{1-\beta}(1+\omega)^{1-\beta}}{1-\beta}, \quad (12)$$

which becomes zero when the local ionization shifts the upper N cutoff down to the adopted lower threshold.

For the three quasars of the present sample, we have adopted the unbiased quasar redshifts estimated from low ionization lines which are representative of the QSO systemic redshift (Espey et al. 1989; Kühr et al. 1984; Tytler & Fan 1992), and higher than the redshifts deduced by the C IV emission line.

Lyman-limit fluxes at the observed frequencies f_ν are derived from the continuum magnitude m_{1450} and the power-law spectral indices of Tytler & Fan (1992). We have found $f_\nu = 8.21$, 2.75, and 5.28 (in unit of 10^{-27} ergs s^{-1} cm^{-2} Hz^{-1}) for the quasars 1101−264, 2126−158, and 0014+813, respectively.

In Figure 6, $\partial n/\partial X_\gamma$ is shown as a function of ω, together with the data points binned as in Bajtlik et al. (1988) for given values of J. Assuming that J does not change in the redshift interval covered by the data and considering lines in the interval $13.3 \le \log N_{\rm H\,I} \le 14.8$, Figure 6 shows that J values outside the range 10^{-22} and 10^{-20} ergs s^{-1} cm^{-2} Hz^{-1} sr^{-1} do not fit the data, while a good fit is obtained assuming the value 7×10^{-22} cgs which is not far from the value derived by the QSO contribution (3×10^{-22} cgs) in the same z interval (Meiksin & Madau 1993). Taking into account slope uncertainties of the faint-end QSO luminosity function and uncertainties in the low-luminosity cutoff, the estimated QSO contribution to the ionizing UVB could be a lower limit and should be considered consistent with the value derived from the proximity effect.

It should be noted that adopting the redshift estimates based on C IV emission lines results in an increase of the UVB of about a factor 2.

It is also worth mentioning that a slight trend is present in the estimates of J for lines with different column densities. Indeed, lines with $\log N_{\rm H\,I} > 14$ are consistent with a value of J higher by a factor 2.5, since they appear more uniformly distributed than weaker lines. While on the one hand such a trend could give important information about the physical structure of the clouds, on the other hand, it should be interpreted, more likely, as a further evidence that lines in the range $15 \le \log N_{\rm H\,I} \lesssim 16$ are blended. In fact, as a first approximation, the line blending does not depend on the quasar vicinity and the column densities of blended saturated features decrease less than what would be expected for a single line by increasing the UV flux.

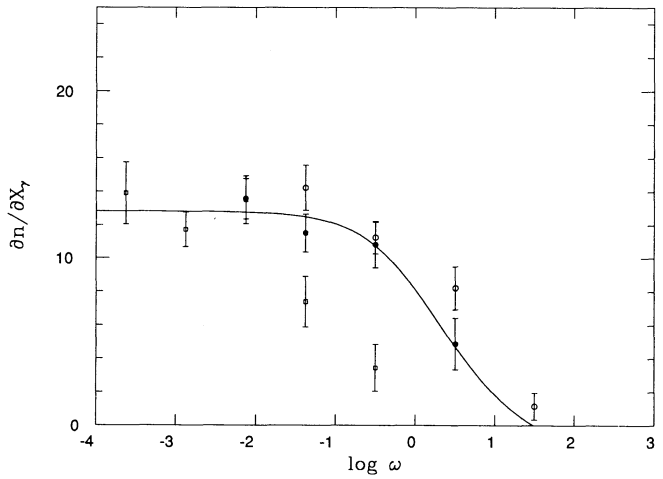

FIG. 6.—$\partial n/\partial X_\gamma$ as a function of log ω. Open circles, filled circles, and open squares correspond to $J_{-22} = 1$, 7, and 100, respectively.

Estimates of the redshift dependence of the UVB await for a larger line sample at high resolution. Nevertheless, we find a good agreement between theory and observations mainly due to the improved values γ and β of the column density distribution derived from a high-resolution sample, and therefore less affected by blending.

6. CONCLUSIONS

A sample of absorption lines has been extracted from the spectrum of PKS 2126−158 ($z_{\rm em} = 3.27$) taken at the resolution of 14 km s^{-1} ($b \simeq 8$ km s^{-1}) over the range $4750 < \lambda < 7000$ Å. The main results are summarized as follows:

1. Besides the five previously known metal systems, we show two new systems, identified by the C IV doublet, and a low-redshift system identified by a Ca II doublet, whose column densities and equivalent width were too weak to be detected in previous observations. A complex velocity structure has been revealed in three of them, with Δv in the range 65–300 km s^{-1}.

2. The Lyα sample not associated with identified metal systems has a considerable fraction of narrow lines: 36% with $b < 20$ km s^{-1}, and 22% with $10 < b < 20$ km s^{-1}. Moreover, a deficit of isolated lines with $b < 20$ km s^{-1} and $\log N_{\rm H\,I} > 13.5$ is found in our spectrum. Thus either they are really absent, or they are systematically hidden in blends.

3. A simple fit in terms of power laws to the distribution of lines as a function of redshift and column density provides the values $\gamma = 2.1$ and $\beta = 1.7$ for the respective exponents. The evolution is lower than found using low-resolution data where a higher value of γ is connected with the apparent faster evolution of stronger lines due to blending.

4. The single–power-law distribution represents a poor fit to the column density distribution. A better fit is obtained with a flatter power-law in the range $13.3 \lesssim \log N_{\rm H\,I} \lesssim 15$ with $\beta \simeq 1.5$. A steeper value $\beta \sim 2$ is found in the same interval for lines with $b \le 20$ km s^{-1} consistently with a deficit of strong lines with low b values. The reality of stronger lines is doubtful, and in any case their distribution appears steeper beyond log

$N_{HI} \sim 15$, with $\beta \sim 2$. A feature at $\log N_{HI} \sim 15$ is predicted by theoretical cloud models in which the potential well due to nonbaryonic dark matter is important.

5. We have reformulated the number density evolution along the line of sight separating explicitly the evolutions of (i) the cloud column density, (ii) the geometrical cross section, and (iii) the cloud number per comoving volume. For simple models of clouds, pressure-confined by an adiabatically expanding IGM, the evolution can be entirely explained by their expansion. However different hypotheses on the change in cosmic time of the diffuse IGM properties and/or the UV background flux may imply a substantial evolution of the cloud volume density in the observed range of redshifts.

6. The effect of breaks or cutoffs has been included in the analysis of the proximity effect. New unbiased redshifts and Lyman limit continuum fluxes have been used. A value for the ultraviolet background flux $J = 7 \times 10^{-22}$ ergs s^{-1} cm^{-2} Hz^{-1} sr^{-1} has been found in the redshift interval $1.8 \lesssim z \lesssim 3.4$. This value is consistent with the integrated QSO contribution to the UVB.

We thank S. D'Odorico for his valuable suggestions. We are grateful to R. Hunstead, P. Petitjean, and S. Savaglio for discussions and to M. Benedettini who performed part of the statistical calculations. We thank also an anonymous referee for useful remarks and suggestions.

REFERENCES

Atwood, B., Baldwin, J. A., & Carswell, R. F. 1985, ApJ, 292, 58
Bajtlik, S., Duncan, R. C., & Ostriker, J. P. 1988, ApJ, 327, 570
Banse, K., Ponz, D., Ounnas, Ch., Grosbol, P., & Warmels, R. 1988, in Instrumentation for Ground-Based Optical Astronomy: Present and Future, ed. L. B. Robinson (New York: Springer-Verlag), 431
Barcons, S., & Webb, J. K. 1991, MNRAS, 253, 207
Bechtold, J., Green, R. F., & York, D. G. 1987, ApJ, 312, 50
Bechtold, J., Weymann, R. J., Lin, Z., & Malkan, M. A. 1987, ApJ, 315, 180
Blades, J. C. 1988, in Quasar Absorption Lines, ed. C. Blades et al. (Cambridge: Cambridge Univ. Press)
Burstein, D., & Heiles, C. 1982, AJ, 87, 1165
Carswell, R. F., Lanzetta, K. M., Parnell, H. C., & Webb, J. K. 1991, ApJ, 371, 36
Carswell, R. F., Morton, D. C., Smith, M. G., Stockton, A. N., Turnshek, D. A., & Weymann, R. J. 1984, ApJ, 278, 486
Carswell, R. F., Webb, J. K., Baldwin, J. A., & Attwood, B. 1987, ApJ, 319, 709
Chaffee, F. H., Jr., Weymann, R. J., Latham, D. W., & Strittmatter, P. A. 1983, ApJ, 267, 12
D'Odorico, S. 1990, Messenger, 61, 51
Duncan, R. C., Vishniac, E. T., & Ostriker, J. P. 1990, ApJ, 368, L1
Espey, B. R., Carswell, R. F., Bailey, J. A., Smith, M. G., & Ward, M. J. 1989, ApJ, 342, 666
Giallongo, E. 1991, MNRAS, 251, 541
Giallongo, E., Cristiani, S., Fontana, A., & Trèvese, D. 1992a, Messenger, 69, 52
Giallongo, E., Cristiani, S., & Trèvese, D. 1992b, ApJ, 398, L9
Gunn, J. E., & Peterson, B. A. 1965, ApJ, 142, 1633
Ikeuchi, S., & Ostriker, J. P. 1986, ApJ, 301, 522
Ikeuchi, S., & Turner, E. L. 1991, ApJ, 381, L1
Kühr, H., McAlary, C. W., Rudy, R. J., Strittmatter, P. A., & Rieke, G. H. 1984, ApJ, 284, L5
Liu, X. D., & Jones, B. J. T. 1988, MNRAS, 230, 481
Lu, L., Wolfe, A. M., & Turnshek, D. A. 1991, ApJ, 367, 19
Lynds, C. R. 1971, ApJ, 164, L73
Madau, P. 1992, ApJ, 389, L1
Meiksin, A., & Madau, P. 1993, ApJ, 403, 690
Meyer, D. H., & York, D. G. 1987, ApJ, 315, L5
Morton, D. C. 1991, ApJS, 77, 119
Murdoch, H. S., Hunstead, R. W., Pettini, M., & Blades, J. C. 1986, ApJ, 309, 19
Ostriker, J. P., & Ikeuchi, S. 1983, ApJ, 268, L63
Peterson, B. A. 1978, in IAU Symp. 79, The Large Scale Structure of the Universe, ed. M. S. Longair, & J. Einasto (Dordrecht: Reidel), 389
Petitjean, P., Bergeron, J., Carswell, R. F., & Puget, J. L. 1993, MNRAS, in press
Petitjean, P., Webb, J. K., Rauch, M., Carswell, R. F., & Lanzetta, K. 1992, MNRAS, in press
Pettini, M., Hunstead, R. W., Smith, L. J., & Mar, D. P. 1990, MNRAS, 246, 545
Rauch, M., Carswell, R. F., Chaffee, F. H., Foltz, C. B., Webb, J. K., Weymann, R. J. Bechtold, J., & Green, R. F. 1992, ApJ, 390, 387
Rees, M. J. 1992, First Light in the Universe: Stars or QSOs?, ed. B. Rocca-Volmerange et al. (Gif-sur-Yvette: Editions Frontières), in press
Sargent, W. L. W., Boksenberg, A., & Steidel, C. C. 1988, ApJS, 68, 539
Sargent, W. L. W., Steidel, C. C., & Boksenberg, A. 1990, ApJ, 351, 364
Sargent, W. L. W., Young, P. J., Boksenberg, A., & Tytler, D. 1980, ApJS, 42, 41
Savage, B. D., & Mathis, J. S. 1979, ARA&A, 17, 73
Smette, A., Surdej, J., Shaver, P. A., Foltz, C. B., Chaffee, F. H., Weymann, R. J., Williams, R. E., & Magain, P. 1992, ApJ, 389, 39
Steidel, C. C., & Sargent, W. L. W. 1987, ApJ, 318, L11
Stone, R. P. S., & Baldwin, J. A. 1983, MNRAS, 204, 347
Trèvese, D., Giallongo, E., & Camurani, L. 1992, ApJ, 398, 491
Tytler, D., & Fan, X-M. 1992, ApJS, 79, 1
Young, P. J., et al. 1979, ApJ, 229, 891